Article

Design and Optimization of Linear Permanent Magnet Vernier Generator for Direct Drive Wave Energy Converter

Mei Zhao [1], Zhiquan Kong [1], Pingpeng Tang [1,*], Zhentao Zhang [2], Guodong Yu [1], Huaqiang Zhang [1], Yongxiang Xu [1] and Jibin Zou [1]

[1] School of Electrical Engineering and Automation, Harbin Institute of Technology, Harbin 150001, China; zhaomei@hit.edu.cn (M.Z.); zhiquankong@hotmail.com (Z.K.); yuguodong@hit.edu.cn (G.Y.); zhq@hit.edu.cn (H.Z.); xuyx@hit.edu.cn (Y.X.); zoujibin@hit.edu.cn (J.Z.)

[2] State Grid Hangzhou Power Supply Company, Hangzhou 310000, China; zzt1075142694@outlook.com

* Correspondence: tpp@hit.edu.cn; Tel.: +86-180-0719-6013

Abstract: A novel linear permanent magnet vernier generator (LPMVG) for small-power off-grid wave power generation systems is proposed in this paper. Firstly, in order to reduce the cogging force and the inherent edge effect of the linear generator, a staggered tooth modular structure is proposed. Secondly, in order to improve the output power and efficiency of the LPMVG and reduce the fluctuation coefficient of electromagnetic force, the relationship between the parameters of the generator is studied, and a method combining multi-objective optimization and single parameter scanning based on the response surface model and particle swarm optimization algorithm is proposed to obtain the optimal structural parameters of the generator. Thirdly, the output power and efficiency of the optimized generator are calculated and analyzed based on the two-dimensional finite element method, and the effectiveness of the multi-objective optimization design method based on the response surface model and particle swarm optimization algorithm is verified. Finally, a prototype is developed, and the calculated results and the measured results are shown to be in good agreement.

1. Introduction

Traditional fossil energy releases greenhouse gases such as carbon dioxide in the process of consumption, causing environmental problems. It has become a top priority to vigorously develop and research renewable energies such as wave energy, solar energy, and wind energy. As the most potentially valuable form of renewable energy, the importance of wave energy is self-evident [1]. The current wave power generation system faces problems such as the use of complex conversion devices, low power density, high costs, and difficult maintenance. In order to improve the efficiency of wave energy, the direct-drive wave power generation system is adopted, which eliminates the growth rate, hydraulic energy storage, and other mechanisms, and reduces the size, weight, and cost of wave energy conversion equipment [2,3].

In recent years, many scholars have studied the wave energy generator. The primary permanent magnet vernier hybrid linear generator for wave power generation was invented and developed in [4]. The fault-tolerant modular primary permanent magnet linear generator was proposed; this generator has the advantages of simple secondary structure, low cogging force, good sinusoidal voltage waveform during power generation, and good power generation characteristics at low speed [5,6]. It is especially suitable for direct drive wave power generation. The novel partitioned stator flux-reversal linear generator is proposed for the linear direct drive wave power generation system. The new structure has low cogging force, high permanent magnet utilization, and high efficiency under load [7]. A novel linear permanent magnet vernier generator suitable for low speeds is proposed,

which is composed of a tubular stator and a tubular translator. The generator can offer the advantages of high-force density and large no-load EMF [8].

In this paper, the staggered tooth module LPMVG is proposed. Based on the principle of magnetic field modulation, the generator generates a harmonic magnetic field with rapid change, has the characteristics of low speed and high thrust, and improves the power density. The staggered tooth modular of LPMVG is proposed in order to reduce the cogging force and the inherent edge end effect of the wave generator. The working principle of modularization is analyzed, and the formula of edge force is derived. The influence of a staggering angle on generator output characteristics is simulated and analyzed, and the optimal staggering angle is determined. Multi-objective optimization is adopted to optimize the output power, efficiency, and electromagnetic force fluctuation coefficient of the staggered tooth module LPMVG. The output power, efficiency, and electromagnetic force fluctuation coefficient before and after optimization are compared, and the optimal results are selected as the structural parameters of the generator. Comparing the output performance of the generator before and after optimization, the effectiveness of the optimization method based on particle swarm optimization and single parameter scanning is verified.

2. Principle and Deign of Generator

2.1. Structural Parameters of LPMVG

This paper proposes a bilateral linear permanent magnet vernier generator, as shown in Figure 1. The generator adopts the double secondary mode, which makes the unilateral normal forces at both ends offset each other and fundamentally eliminates the adverse factors of the normal force on the generator [9].
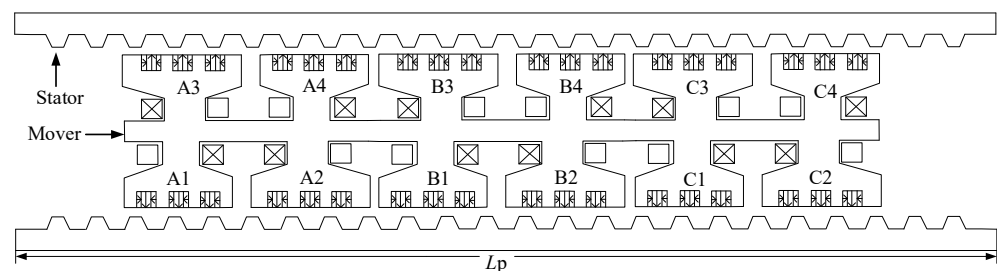
Figure 1. Bilateral linear permanent magnet vernier generator.

2.2. Working Principle of Generator

It is necessary to make some ideal assumptions before analyzing the working principle of the LPMVG: (1) The hysteresis loss and eddy current loss of the generator are not considered; (2) the influence of core saturation is ignored; (3) the relative permeability of the permanent magnet is consistent with the vacuum permeability. The Fourier series form of the magneto motive force F_{PM} generated by the permanent magnet on the armature tooth can be expressed as:

$$F_{PM}(x) = \sum_{n,odd}^{\infty} F_n \cos\left[np_{PM} \frac{2\pi x}{L_P} \right] \tag{1}$$

where F_n is the harmonic amplitude, L_p is the primary length, and p_{PM} is the effective pole pair of the permanent magnet.

The Fourier form of the total magnetic conductivity of the generator is:

$$\Lambda(x,t) = \Lambda_0 + \sum_{m=1}^{\infty} \Lambda_m \cos\left[mn_t \frac{2\pi}{L_p}(x - v_p t - x_0) \right] \tag{2}$$

where Λ_0 is the amplitude of the fundamental wave of magnetic conductivity; Λ_m is the harmonic amplitude of magnetic conductivity; n_t is the number of secondary effective teeth; and v_p is the primary speed.

The air gap flux density generated by the permanent magnet at the primary teeth of the generator can be expressed as the product of the magneto motive force and the total magnetic conductivity. According to (1) and (2), the air gap flux density of the generator can be expressed as

$$
\begin{aligned}
B(x,t) \quad &= F_{PM}(x)\Lambda(x,t) \\
&= \sum_{n,odd}^{\infty} F_n\Lambda_0 \cos\left[np_{PM}\frac{2\pi x}{L_p}\right] \\
&+ \frac{1}{2}\sum_{n,odd}^{\infty}\sum_{m=1}^{\infty} F_n\Lambda_m \cos\left[\frac{2\pi x}{L_p}(np_{PM}+\mathrm{m}n_t) - \frac{2\pi \mathrm{m}n_t(v_p t+x_0)}{L_p}\right] \\
&+ \frac{1}{2}\sum_{n,odd}^{\infty}\sum_{m=1}^{\infty} F_n\Lambda_m \cos\left[\frac{2\pi x}{L_p}(np_{PM}-\mathrm{m}n_t) + \frac{2\pi \mathrm{m}n_t(v_p t+x_0)}{L_p}\right]
\end{aligned}
\tag{3}
$$

The lower the order of the effective harmonic, the higher the amplitude; so in general, $n = 1$, $m = 1$ is selected, and the polar logarithm of the effective harmonic at this time can be expressed as

$$
p_{1,1} = |p_{PM} - n_t|
\tag{4}
$$

It can be seen from the previous analysis that when the number of harmonic poles generated by the armature winding in the air gap is the same as the number of effective harmonic poles generated by the permanent magnet, the fluctuation of the generator output electromagnetic force is the smallest. There is a certain ratio between the generator effective harmonic speed and the generator primary movement speed, as shown in (5).

$$
v_p = \frac{n_t}{p_{1,1}}v_r = G_t v_r
\tag{5}
$$

As shown in Figure 2, the air gap flux density generated by the permanent magnet in the air gap of the effective length of the generator can be obtained by Fourier decomposition of the air gap flux density. The pole number of the permanent magnet is 18, and a large second harmonic component is also generated in the air gap. The air gap flux density of the generator when only the armature windings is considered is shown in Figure 3. It can be clearly seen from the Fourier decomposition that the second harmonic of the magnetic field generated by the armature winding is the main component and produces a higher 18th harmonic. The effective number of secondary teeth in the generator design is 20. Through simulation analysis, it can be seen that the relationship between the three satisfies (4). At the same time, it also proves that the air gap magnetic field of the generator is jointly affected by the permanent magnet and armature winding during operation, and it also proves the correctness of the magnetic field modulation principle.

(a)

(b)
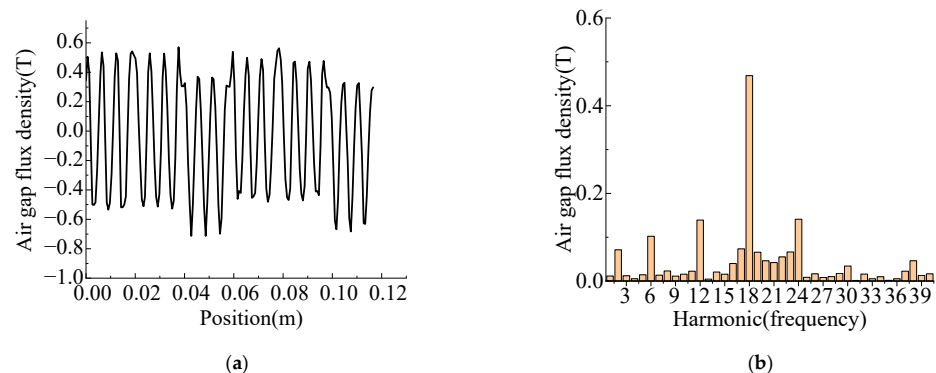
Figure 2. Analysis of air gap flux density and harmonic generated by permanent magnet array: (**a**) Air gap magnetic density (**b**) Harmonic content in air gap.
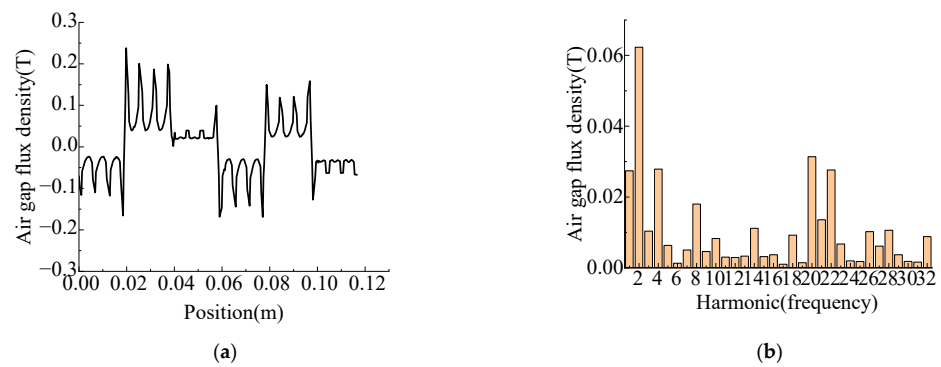
Figure 3. Analysis of air gap flux density and its harmonic generated by armature winding: (**a**) Air gap magnetic density (**b**) Harmonic content in air gap.

3. Design of Staggered Tooth Modular Generator

3.1. Structure of Modular LPMVG

A modular structure is proposed to reduce the cogging force of the linear permanent magnet vernier wave generator [10].

3.2. Cogging Force of Actuator Modularization

The edge force of each module of the generator is as follows

$$\begin{cases} F_{A\_end} = \sum\limits_{n=1}^{\infty} F_n \sin(2n\pi \frac{x}{\tau_s}) \\ F_{B\_end} = \sum\limits_{n=1}^{\infty} F_n \sin(2n\pi \frac{x}{\tau_s} + \frac{2\pi}{3}) \\ F_{C\_end} = \sum\limits_{n=1}^{\infty} F_n \sin(2n\pi \frac{x}{\tau_s} - \frac{2\pi}{3}) \end{cases} \tag{6}$$

where n is the number of harmonics, x is the relative position of the secondary and primary teeth, and τ_s is the pole pitch of the secondary tooth. Therefore, the total edge cogging force of the LPMVG is the sum of three module cogging forces, and can be expressed by

$$F_{total\_end} = F_{A\_end} + F_{B\_end} + F_{C\_end} \tag{7}$$

3.3. Modular Simulation Verification

The simulation results of cogging force and total cogging force of each module of the LPMVG are shown in Figure 4. It can be seen that the peak-to-peak cogging force is reduced from 377 N to 135 N, and the cogging force is greatly reduced.
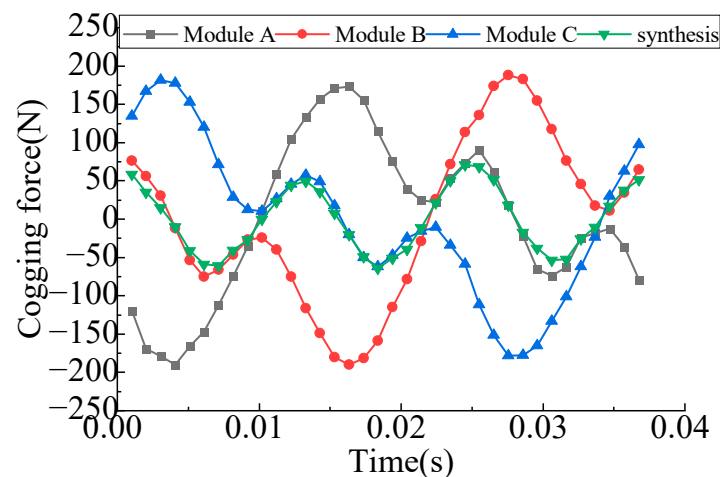
Figure 4. Modular principle verification diagram.

The simulation results are shown in Figures 5–7. It can be seen that when the no-load back EMF is basically unchanged, the peak-to-peak cogging force is reduced from 216 N to 135 N, and the waveform distortion rate is changed from 13.06% to 4.85%, which greatly improves the performance of the generator.
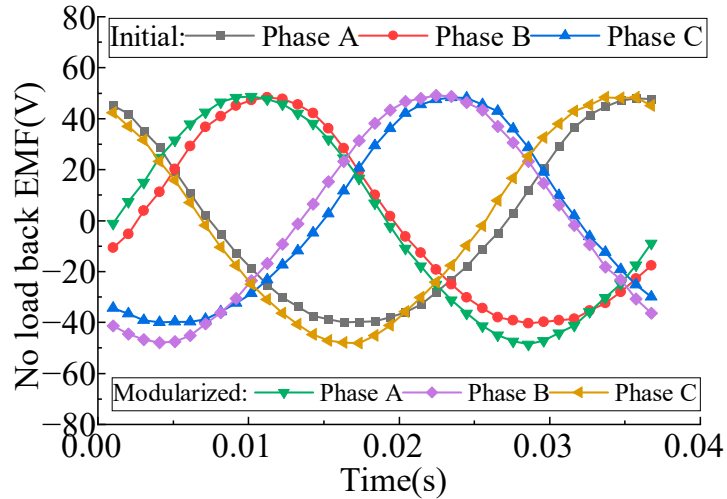
Figure 5. The waveform of no-load back EMF.
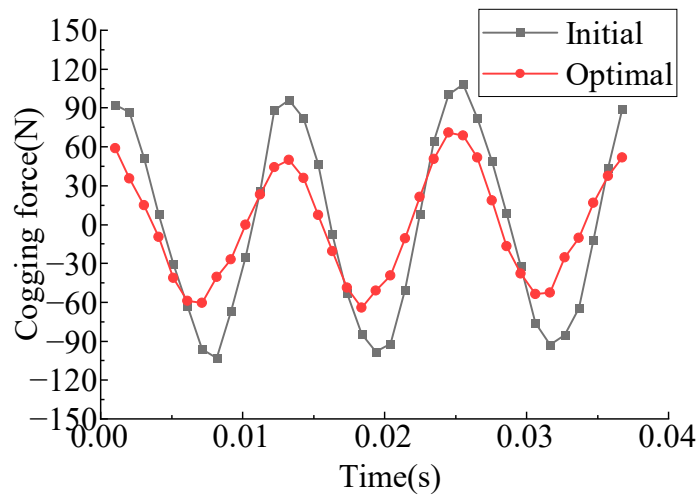
Figure 6. The waveform of cogging force.
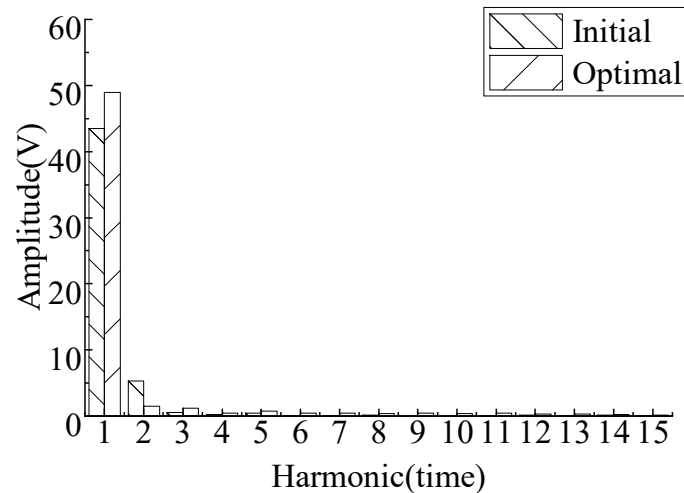
Figure 7. Comparison of harmonic.

3.4. Optimal Design and Analysis of Secondary Staggered Tooth

As shown in Figure 8, the staggered tooth LPMVG was proposed based on the original modular LPMVG in order to lower the peak-to-peak cogging force of the LPMVG. The bilateral secondary tooth is staggered by a certain distance, which causes the primary tooth permanent magnet array to be staggered by a certain phase. The phase difference can be expressed as "$d\cdot\pi/\tau$". The simulation results of cogging force, no-load back EMF, and output power and efficiency of the generator are shown in Table 1. Finally, considering the output power, no-load back EMF, cogging force, normal force, and efficiency of the generator, the bilateral tooth staggering angle of the generator is selected as 30°.
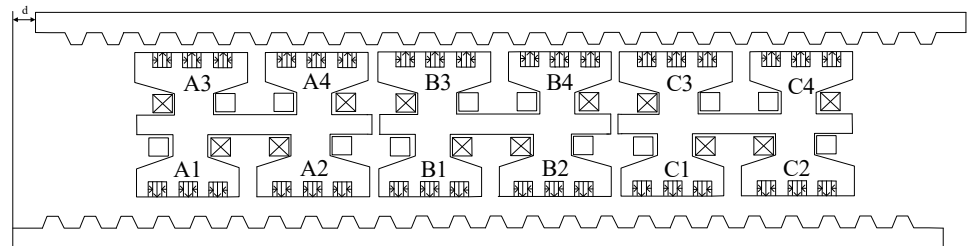
Figure 8. Staggered tooth bilateral linear permanent magnet vernier generator.

Table 1. Generator performance at different stagger angles.

Stagger Angle	EMF (V)	Cogging Force (N)	Output Power (W)	Efficiency (%)
0°	49.327	130.106	50.816	78.86
15°	49.037	124.169	49.49	78.81
30°	47	94.076	46.868	78.88
45°	45.578	65.87	42.624	78.84
60°	43.073	28.175	37.148	78.69

4. Multi-Objective Optimization of Staggered Tooth Module LPMVG (STMLPMVG)

4.1. Topology and Simulation Variables

As shown in Figure 9, 11 design variables of the STMLPMVG are presented in this paper, which also includes other constant structural parameters related to the generator. The multi-objective optimization flow chart is shown in Figure 10. The definition, initial value, and variation range of each design variable are shown in Table 2. Table 3 shows the structural parameters of the STMLPMVG that remain unchanged.
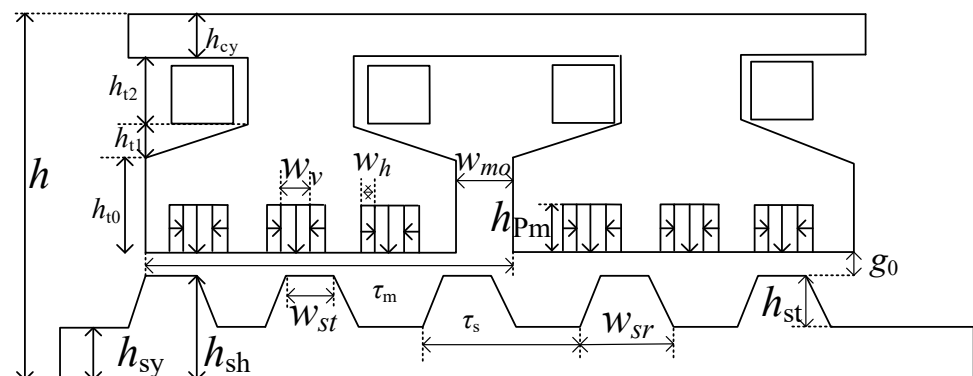
Figure 9. Dimension structure of STMLPMVG.
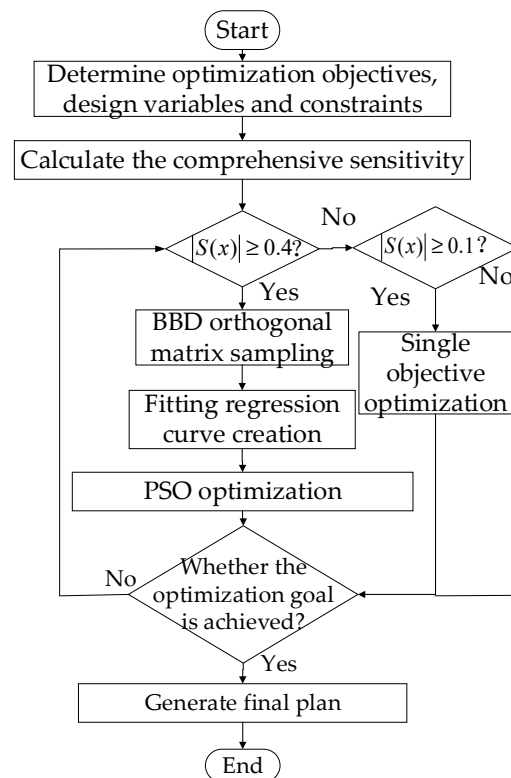
Figure 10. Multi-objective optimization flow chart.

Table 2. Optimization variables of STMLPMVG.

Variable	Definition	Initial Value	Variation Range
w_v	Longitudinal permanent magnet length	4 mm	4~6 mm
w_h	Length of transverse permanent magnet	3 mm	2~4 mm
K_{bp}	Ratio of secondary tip w_{st} to secondary pole τ_s	0.3	0.2~0.4
K_{bt}	Ratio of secondary tooth end w_{sr} to secondary pole τ_s	0.5	0.4~0.6
K_{ph}	Ratio of secondary tooth height h_{st} to secondary height h_{sh}	0.5	0.4~0.6
h_{pm}	PM thickness	4 mm	3~5 mm
w_{mo}	Primary slot opening width	2 mm	1~3 mm
h_{t0}	Primary slot opening height	10 mm	6~12 mm
h_{t1}	Primary slot wedge height	4 mm	3~5 mm
h_{t2}	Primary slot height	15 mm	13~17 mm
h_{cy}	Primary yoke thickness	10 mm	7~11 mm

Table 3. Constant structural parameters.

Invariant Parameter	Definition	Initial Value
L_{ar}	Effective length of generator	298 mm
τ_m	Primary slot pitch	52.45 mm
τ_s	Secondary pole pitch	14.7 mm
g_0	Air gap width	1 mm

4.2. Sensitivity Analysis and Calculation

4.2.1. Determination of Optimization Objective

In order to improve the generator performance, the maximum value of output power and efficiency and the minimum value of electromagnetic force fluctuation coefficient are

taken as the optimization objective for the multi-objective optimization. The output power can be expressed as

$$P_0 = U_{\text{out}} I_{\text{out}} = 3 \frac{U_0}{\sqrt{2}} \frac{I_0}{\sqrt{2}} = 1.5 U_0 I_0 \tag{8}$$

where U_m and I_m are the amplitudes of generator voltage and current.

Power generation efficiency is the ratio of output power to input power, which is also an important index to reflect the wave energy generation capacity and the energy conversion efficiency of generators. The generation efficiency formula of the generator is:

$$\eta = \frac{P}{P_{in}} \times 100\% = \frac{P}{P + P_{Cu} + P_{Fe}} \times 100\% \tag{9}$$

where P_{in} is the input power of generator, P is the output power of generator, P_{Cu} is the generator copper loss, and P_{Fe} is the generator iron loss.

The fluctuation coefficient is the ratio of the peak value of electromagnetic force to the average electromagnetic force. The staggered tooth module LPMVG works in a severe marine environment. The fluctuation coefficient can reflect the reliability of the generator in a difficult environment. It is one of the important indicators of the generator. The formula is defined as follows

$$\gamma = \frac{F_{\text{max}} - F_{\text{min}}}{F_{\text{av}}} \tag{10}$$

where F_{max} is the maximum value of electromagnetic force, F_{min} is the minimum value of electromagnetic force, and F_{av} is the average value of electromagnetic force.

4.2.2. Calculation and Analysis of Sensitivity

There are 11 independent optimization variables of the STMLPMVG. If the BBD orthogonal matrix method is directly used, 177 discrete variables are also required. The simulation time is too long. The sensitivity analysis method is used to reduce the simulation time, increase efficiency, and improve the optimization accuracy of multi-objective optimization. The sensitivity calculation formula can be expressed as follows

$$G(n_{\text{i}}) = \frac{\partial g(n_{\text{i}})}{\partial n_{\text{i}}} = \frac{\Delta g(n_{\text{i}}) / g(n_{\text{i}})}{\Delta n_{\text{i}} / n_{\text{i}}} \tag{11}$$

Each design variable has a different effect on the optimization target, and the comprehensive sensitivity of the motor is calculated by ranking and weighting the importance of the optimization target. The calculation formula of comprehensive sensitivity is as follows [11]

$$s(n_{\text{i}}) = \lambda_1 |G_{\text{P}_0}| + \lambda_2 |G_\eta| + \lambda_3 |G_{\text{F}_\text{r}}| \tag{12}$$

where λ_1, λ_2, and λ_3 are the weight coefficients, and the sum of the three is one. G_{P_0}, G_η, and G_{F_r} are the sensitive factors of the design variable n_{i} to the optimized target output power, generation efficiency, and electromagnetic force fluctuation.

The comprehensive sensitivity value shown in Table 4 and Figure 11 can be obtained according to (12). The design variables of significant sensitivity for a comprehensive sensitivity value greater than 0.4 contain the longitudinal magnetized permanent magnet width, radial magnetized permanent magnet width, permanent magnet thickness, and primary slot width. The comprehensive sensitivity value that is greater than 0.1 and less than 0.4 is taken as the general sensitivity; that is, the tooth width coefficient of the secondary tooth, the height of the primary slot, and the height of the primary slot opening are the design variables of general sensitivity. Finally, the sensitivity value that is less than 0.1 is regarded as insignificant sensitivity. Therefore, the multi-objective optimization algorithm is used to obtain the optimal design value for the significant sensitivity, the single objective optimization method is used to optimize the general sensitivity, and the initial value can be used for the non-significant sensitivity variable without optimization, so as to obtain the final result.

Table 4. Sensitivity values of three design variables.

Variable	G_P	G_η	G_γ	$S(n_i)$
w_v	−0.442	-0.038	−1.535	0.649
w_h	−0.862	−0.039	−1.227	0.725
K_{bp}	−0.064	−0.001	0.786	0.262
K_{bt}	−0.033	0.011	−0.090	0.044
K_{ph}	−0.032	0.006	0.076	0.037
h_{pm}	0.880	−0.009	−0.302	0.445
w_{mo}	0.385	−1.303	0.030	0.554
h_{t0}	−0.274	−0.008	0.357	0.219
h_{t1}	−0.111	−0.023	−0.040	0.063
h_{t2}	0.007	0.032	0.115	0.047
h_{cy}	0.008	0.005	0.040	0.017
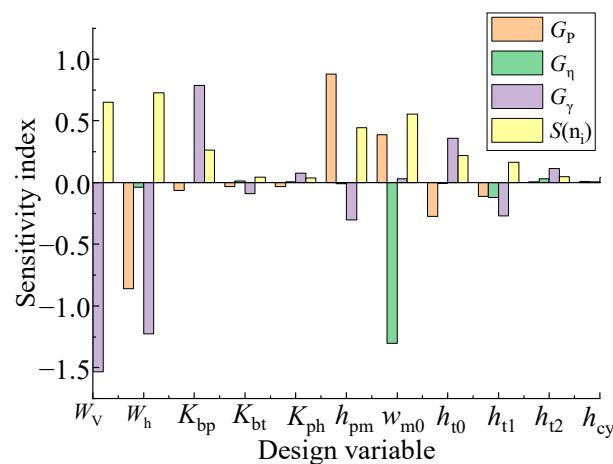
Figure 11. Sensitivity index of design variables.

4.3. BBD Orthogonal Experimental Matrix

The Box−Behnken design (BBD) method is a comprehensive DoE method used to establish RS models which are suitable for 2–5 design variables [12]. The BBD method is encoded by three factors, namely −1, 0, and 1, where −1 is the low level factor, 0 is the center point factor, and 1 is the high level factor. There are four significant sensitivity design variables for the STMLPMVG, and the values of design variables at each level are shown in Table 5 [13]. The BBD orthogonal matrix is shown in Table 6. There are 29 experiments in total, and the number of experiments for the four design variables is $3^4 = 81$. It can be seen that the BBD orthogonal matrix can effectively reduce the number of experiments and simulation time [14].

Table 5. Design variable level value.

Level	w_v (mm)	w_h (mm)	h_p (mm)	w_{m0} (mm)
−1	4	3	4	1.5
0	4.5	3.5	4.5	2
1	5	4	5	2.5

Table 6. BBD orthogonal test matrix.

Order Number	w_v	w_h	h_{pm}	w_{m0}	P (W)	η (%)	γ
1	4.5	3	4.5	1.5	47.97	78.342	0.351
2	4.5	3.5	5	2.5	48.39	78.339	0.308
3	4.5	3.5	4.5	2	41.23	78.129	0.344

Table 6. *Cont.*

Order Number	w_V	w_h	h_{pm}	w_{m0}	P (W)	η (%)	γ
4	4	3.5	4.5	2.5	48.50	78.65	0.381
5	4.5	3.5	4	1.5	32.46	77.55	0.475
6	4.5	4	4.5	1.5	21.70	75.74	0.777
7	4.5	3.5	4.5	2	41.23	78.135	0.344
8	4.5	3.5	4.5	2	41.05	78.041	0.35
9	4.5	3.5	4	2.5	38.72	78.246	0.45
10	4	3.5	4	2	40.34	78.417	0.566
11	4	3.5	5	2	50.72	78.548	0.399
12	4.5	4	5	2	27.06	76.27	0.69
13	4	3.5	4.5	1.5	40.89	78.141	0.32
14	5	3.5	4.5	1.5	30.83	76.95	0.574
15	4.5	3.5	4.5	2	41.23	78.126	0.344
16	4	4	4.5	2	30.31	77.31	0.465
17	4.5	3.5	4.5	2	41.05	78.041	0.35
18	4.5	3	5	2	59.65	78.9	0.245
19	4.5	3	4	2	48.51	78.782	0.247
20	5	3.5	4.5	2.5	36.49	77.59	0.475
21	5	3	4.5	2	51.72	78.647	0.305
22	4	3	4.5	2	52.67	78.855	0.697
23	5	4	4.5	2	20.34	75.86	0.877
24	4.5	3.5	5	1.5	40.92	77.8	0.375
25	4.5	4	4.5	2.5	25.57	76.47	0.68
26	4.5	3	4.5	2.5	57.63	78.998	0.228
27	5	3.5	4	2	30.27	77.257	0.613
28	5	3.5	5	2	38.1	77.44	0.53
29	4.5	4	4	2	20.97	76.09	0.584

4.4. Surface Response Analysis

The second-order polynomial of the RS model can express as

$$G(t) = a_0 + \sum_{i=1}^{4} a_i t_i + \sum_{i=1}^{4} a_{ii} t_i^2 + \sum_{i=1}^{2} \sum_{j>i}^{4} a_{ij} t_i t_j + \varepsilon \tag{13}$$

where *G(t)* is the response value and a_0, a_i, a_{ij}, and a_{ii} are the regression coefficients.

The fitting function of the optimization objective can be obtained by using the simulation data of the 29 models in Table 6. The second-order fitting function of the output power is

$$\begin{aligned} P = \quad &-386.12 + 69.32 w_v + 95.61 w_h + 45.15 h_{pm} + 46.66 w_{m0} - \\ &9.02 w_v w_h - 2.55 w_v h_{pm} - 1.95 w_v w_{m0} - 5.05 w_h h_{pm} - 5.8 w_h w_{m0} \\ &+1.21 h_{pm} w_{m0} - 3.52 w_v^2 - 7.06 w_h^2 - 1.05 h_{pm}^2 - 4.07 w_{m0}^2 \end{aligned} \tag{14}$$

The second-order fitting function of generator efficiency is

$$\begin{aligned} \eta = \quad &+36.76 + 4.82 w_v + 16.16 w_h + 2.13 h_{pm} + 3.07 w_{m0} - \\ &1.24 w_v w_h + 0.05 w_v h_{pm} + 0.13 w_v w_{m0} + 0.06 w_h h_{pm} + 0.07 w_h w_{m0} \\ &-0.16 h_{pm} w_{m0} - 0.22 w_v^2 - 1.92 w_h^2 - 0.23 h_{pm}^2 - 0.65 w_{m0}^2 \end{aligned} \tag{15}$$

The second-order fitting function of the electromagnetic force fluctuation coefficient γ is

$$\begin{aligned} \gamma = \quad &+31.18 - 7.04 w_v - 6.93 w_h - 1.75 h_{pm} + 0.49 w_{m0} + \\ &0.8 w_v w_h + 0.084 w_v h_{pm} - 0.16 w_v w_{m0} + 0.11 w_h h_{pm} + 0.026 w_h w_{m0} \\ &-0.042 h_{pm} w_{m0} + 0.47 w_v^2 + 0.44 w_h^2 + 0.11 h_{pm}^2 + 0.068 w_{m0}^2 \end{aligned} \tag{16}$$

4.5. Particle Swarm Optimization Algorithm

In order to find the global optimal solutions for the three optimization objectives, the method of Particle Swarm Optimization (PSO) is used to optimize the STMLPMVG [15]. The basic equation of PSO can be expressed by

$$\begin{cases} V_{id}^{k+1} = \omega V_{id}^k + c_1 r_1 (P_{id}^k - X_{id}^k) + c_1 r_1 (Q_{id}^k - X_{id}^k) \\ X_{id}^{k+1} = X_{id}^k + V_{id}^{k+1} \end{cases} \tag{17}$$

where V is the particle velocity, X is the population size, ω is inertia weight, c_1 and c_2 are acceleration coefficients, r_1 and r_2 are random numbers of [0, 1], and P and Q are individual and global optimal points.

Through establishing the mathematical model of the STMLPMVG, the fitting curve between the optimization objective and the design variable is obtained, and it is substituted into the optimization objective function which is shown in (18). The global optimal solution set obtained by the particle swarm optimization algorithm is shown in Table 7.

$$g(n_\mathrm{i}) = \omega_1 \frac{g_{P_\mathrm{o}}(n_\mathrm{i})}{P_\mathrm{o}'} + \omega_2 \frac{g_\eta(n_\mathrm{i})}{\eta'} + \omega_3 \frac{K'}{g_K(n_\mathrm{i})} \tag{18}$$

Table 7. Optimization results of design variables and objectives.

Variable	Before Solution	After Solution
w_v (mm)	4	4.5
w_h (mm)	3	3
h_pm (mm)	4	5
w_m0 (mm)	2	2.5
P (W)	47.04	63.05
η (%)	78.78	78.97
γ	0.71	0.222

4.6. Single Objective Optimization of General Sensitivity Variables

Figure 12 shows the relationship between output power and efficiency with the tooth width coefficient of the secondary tooth. It can be seen that the generator efficiency basically does not change much, and the output power first increases and then decreases with the tooth width coefficient of the secondary tooth increasing. As shown in Figure 13, the fluctuation coefficient decreases and then increases with the increase of the tooth width coefficient of the secondary tooth. The fluctuation coefficient reaches the minimum point when the tooth width coefficient of the secondary tooth is 0.3. The tooth width coefficient of the secondary tooth is selected as 0.3 through the comprehensive analysis of Equation (18).

Figure 14 shows the relationship between output power and efficiency with the height of the primary slot opening. It can be seen that the efficiency remains basically unchanged with the increase of the height of the primary slot opening, while the output power decreases with the increase of the height of the primary slot opening. Figure 15 shows the relationship between the fluctuation coefficient and the height of the primary slot opening. The fluctuation coefficient generally shows an upward trend with the height of the primary slot opening increasing. To sum up, the height of the primary slot opening is obtained by 6 mm.

As shown in Figure 16, the efficiency increases with the increase of the height of the primary slot, while the output power first increases and then fluctuates with the increase of the height of the primary slot. Figure 17 shows the relationship between the fluctuation coefficient and the height of the primary slot. The fluctuation coefficient first decreases and then increases with the height of the primary slot increasing. To sum up, the height of the primary slot is obtained by 17 mm.
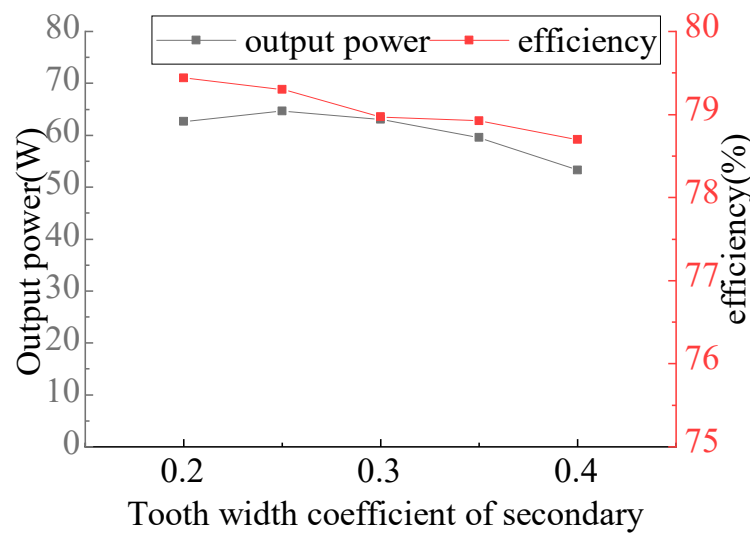
Figure 12. Relationships between output power and efficiency with the tooth width coefficient of the secondary tooth.
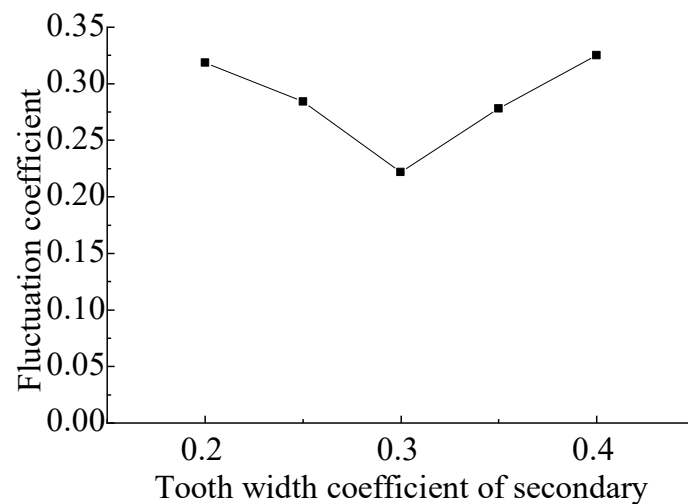
Figure 13. Relationship between electromagnetic force pulsation coefficients and the tooth width coefficient of the secondary tooth.
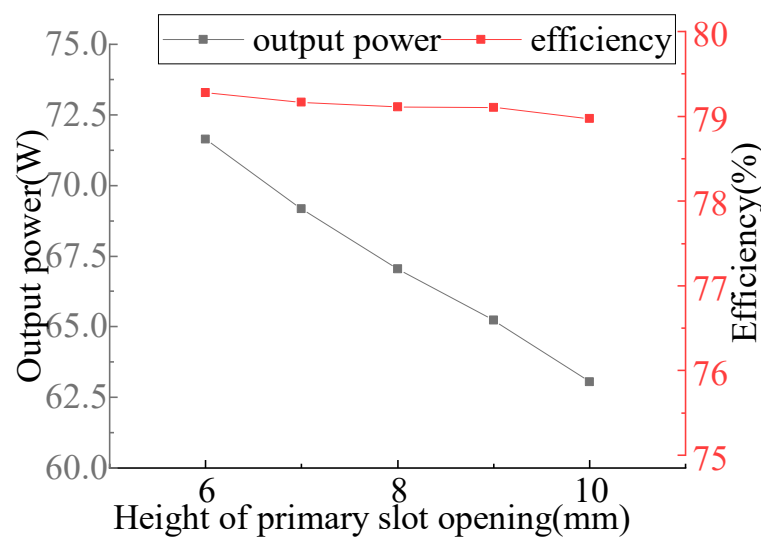
Figure 14. Relationships between output power and efficiency and the height of primary slot opening.
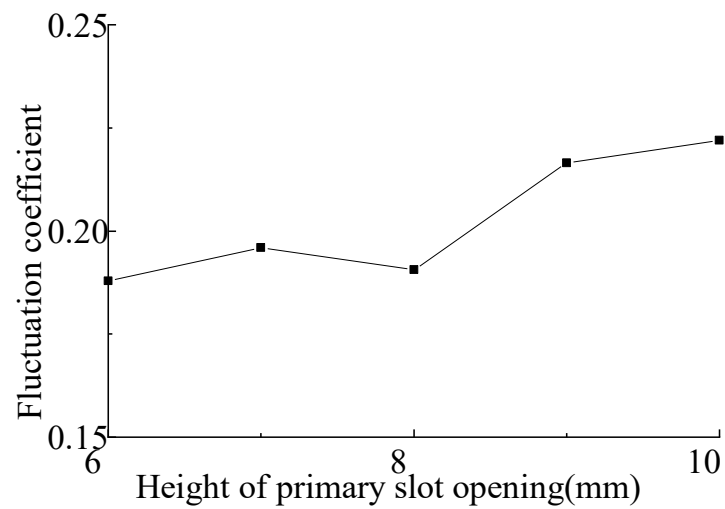
Figure 15. Relationship between electromagnetic force pulsation coefficients and the height of primary slot opening.
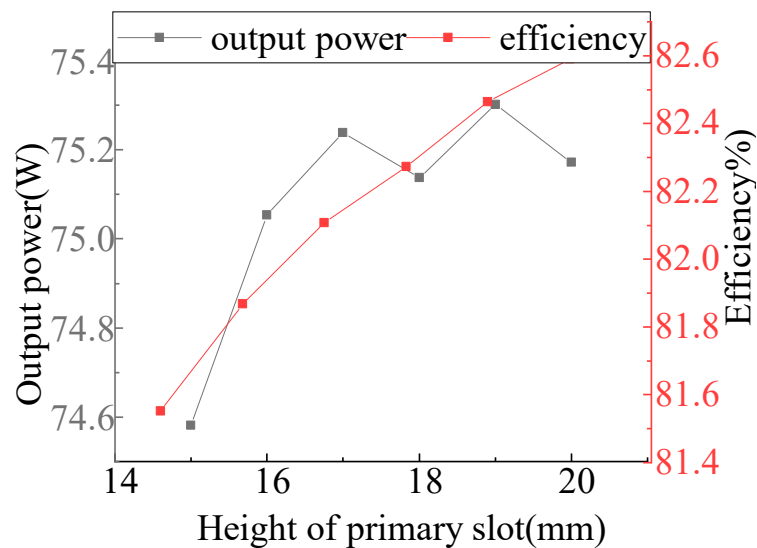
Figure 16. Relationships between output power and efficiency with the height of primary slot.
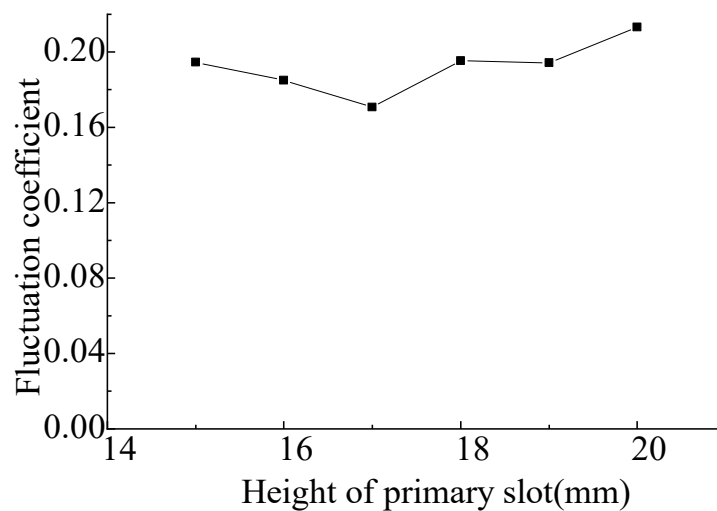
Figure 17. Relationship between electromagnetic force pulsation coefficient and the height of primary slot.

4.7. Final Optimization Results and Comparison

The comparison of design variables and the values of the optimization objectives of the STMLPMVG before and after optimization are shown in Table 8. It can be seen that the amplitude of the load voltage greatly increased after optimization in Figures 18 and 19, while the amplitude of the load current increased. The output power increased from 47.04 W to 75.25 W, and the efficiency of the generator also increased from 78.78% to 82.11%. Figure 20 shows the comparison of electromagnetic force before and after optimization. It can be seen that the electromagnetic force of the optimized STMLPMVG increased from 133 N to 206 N, and the fluctuation coefficient decreased from 0.71 to 0.171.

Table 8. Comparison results of the STMLPMVG.

	Before Solution	After Solution
w_{v} (mm)	4	4.5
w_{h} (mm)	3	3
K_{bp}	0.3	0.3
K_{bt}	0.5	0.5
K_{ph}	0.5	0.5
h_{pm} (mm)	4	5
w_{m0} (mm)	2	2.5
h_{st} (mm)	10	12
h_{t0} (mm)	10	6
h_{t1} (mm)	4	4
h_{t2} (mm)	15	17
h_{cy} (mm)	10	10
P (W)	47.04	75.25
η (%)	78.78	82.11
γ	0.71	0.171
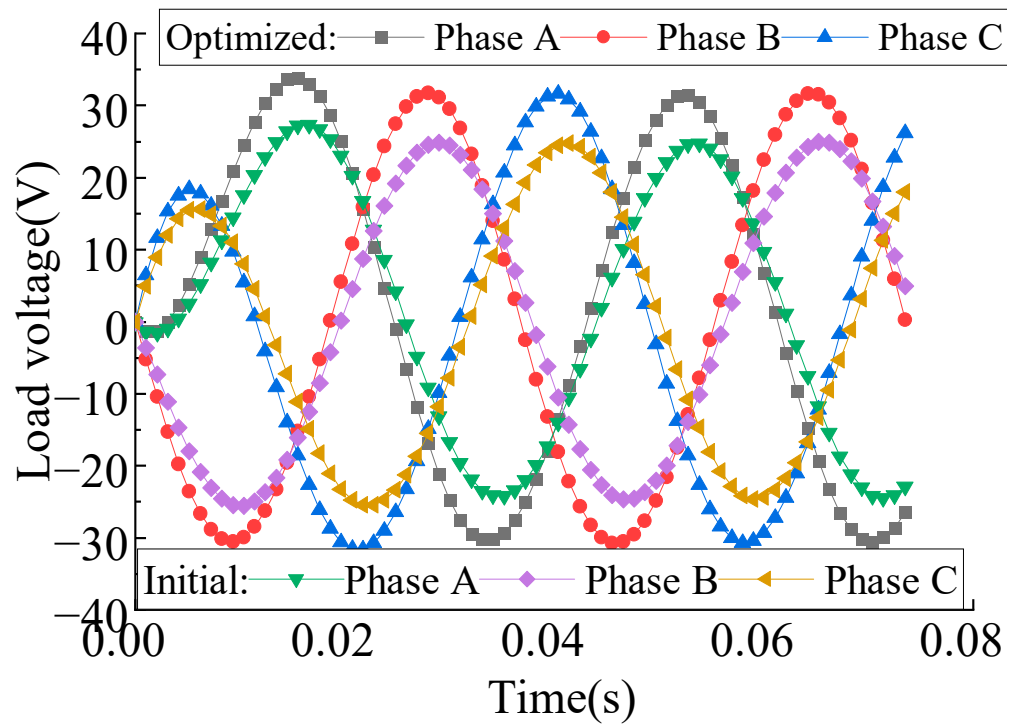
Figure 18. Comparison of load voltage.
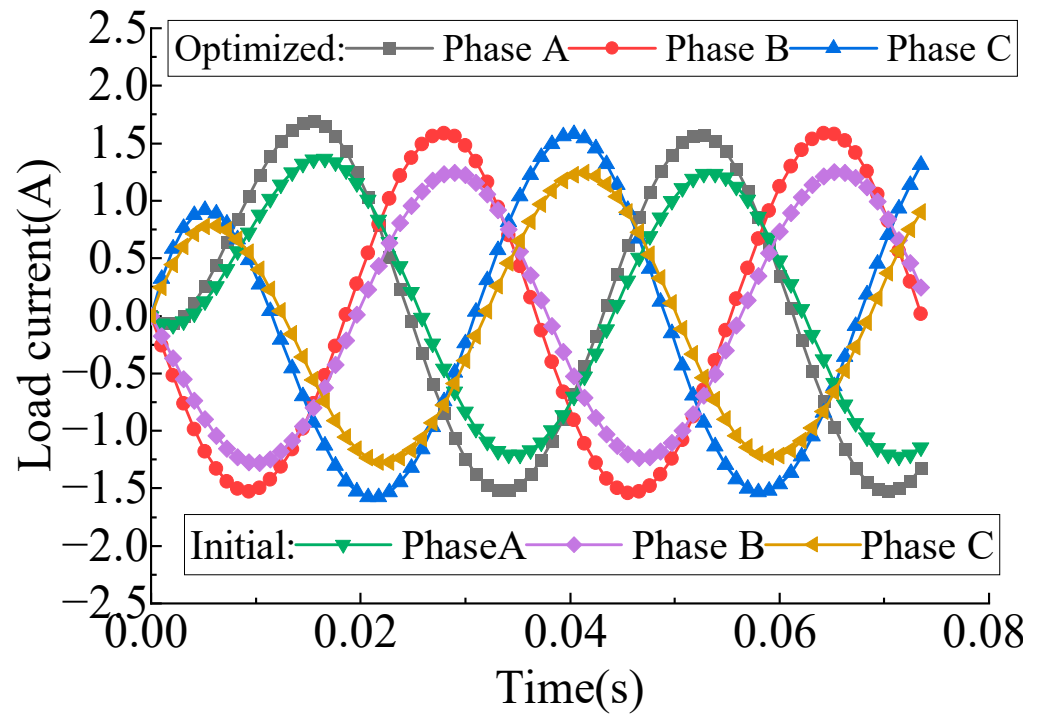
Figure 19. Comparison of load current.
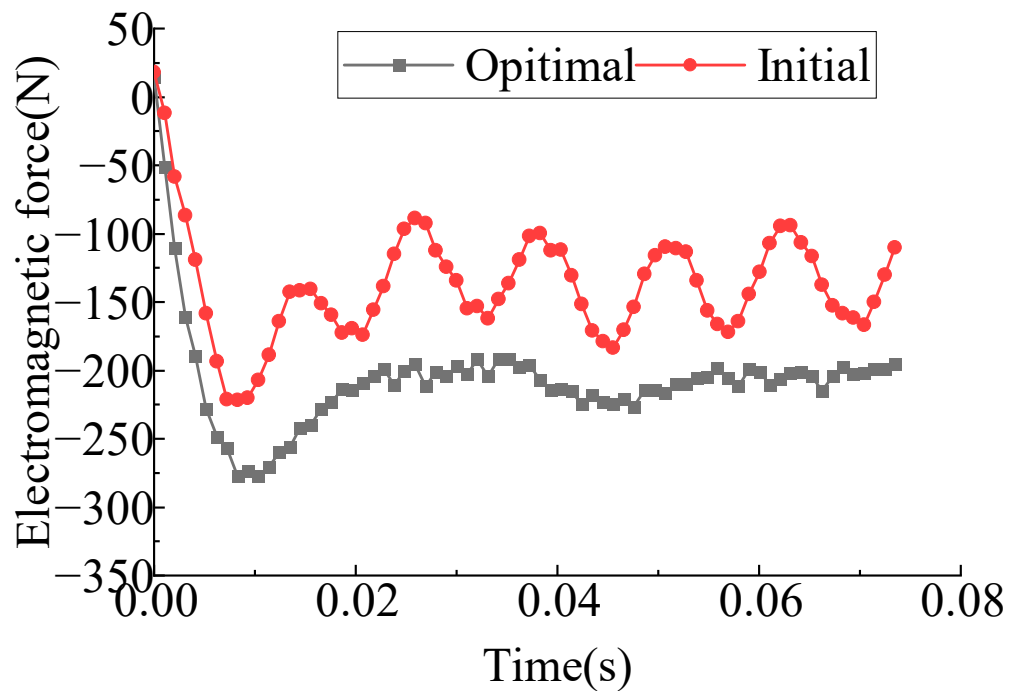
Figure 20. Comparison of electromagnetic force.

5. Exoeriment and Analysis Result

A prototype of the STMLPMVG motor based on the optimized parameters is manufactured. The mover, stator, and machine structure of the prototype motor are shown in Figure 21.

(**a**)   (**b**)   (**c**)
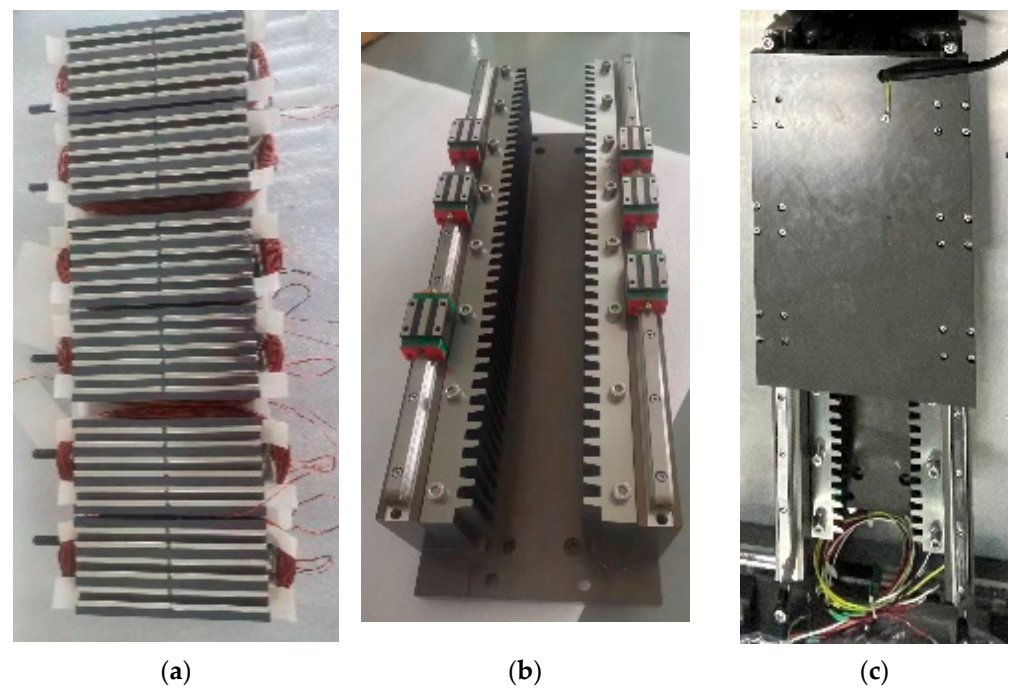
Figure 21. Prototype of STMLPMVG: (**a**) Mover. (**b**) Stator. (**c**) Machine structure.

Figure 22 present the no-load back EMF waveforms of the STMLPMVG varying with time at a speed of 0.4 m/s. It can be seen from Figure 23 that the experimental result is in accord with the result of the FEM.
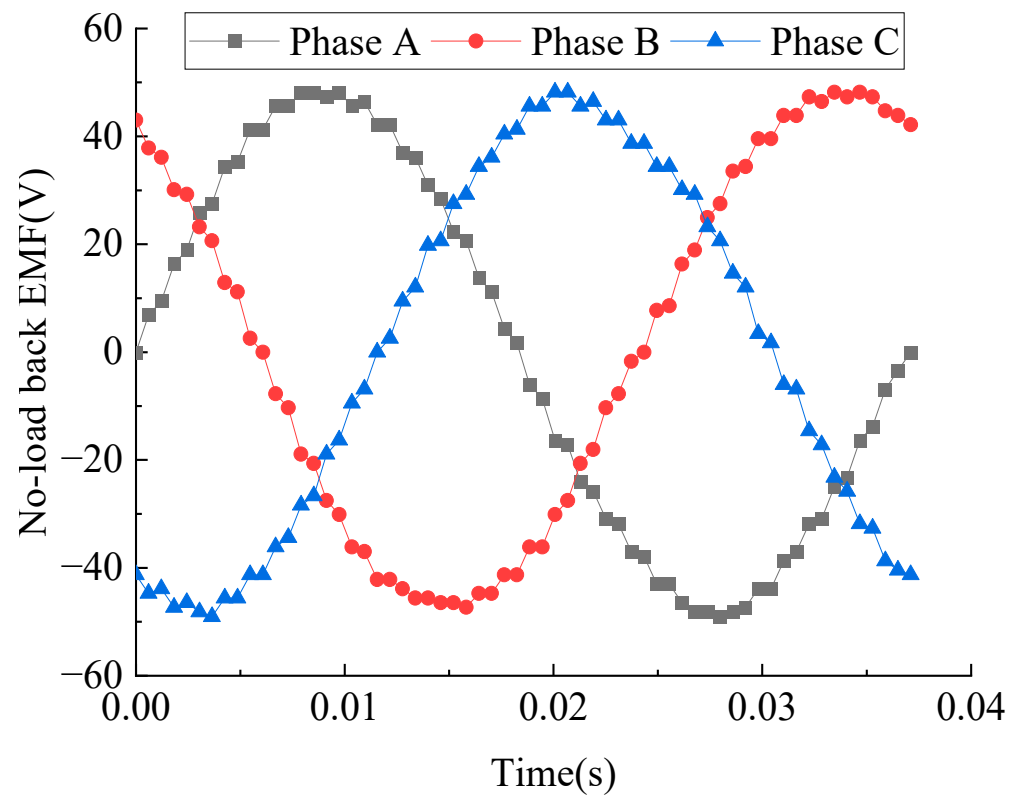
Figure 22. STMLPMVG no-load back EMF.
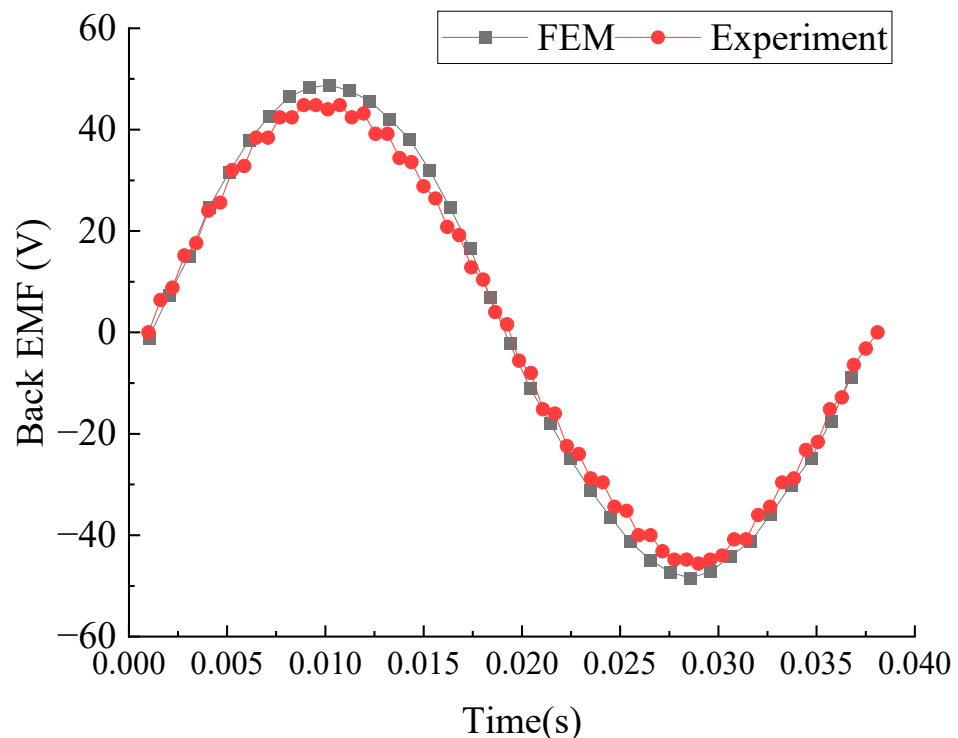
Figure 23. Comparison of waveforms of no-load back-EMF.

6. Conclusions

A novel STMLPMVG for a small-power off-grid wave power generation system was proposed in this paper. The principle of magnetic field modulation was derived, and the correctness of the principle was verified by an analysis of the air gap magnetic density. A comprehensive framework of multi-objective optimization for the STMLPMVG based on a combination of RS models and PSO was proposed. The output power of the STMLPMVG after optimization is increased by 60%, the generation efficiency is increased by 4.2%, and the fluctuation coefficient is reduced by 82.9%. Finally, a prototype of the STMLPMVG was built and the experiment results showed good agreement with the simulation results.

Author Contributions: Conceptualization, M.Z.; Methodology, M.Z.; Software, P.T. and Z.Z.; Validation, P.T.; Formal analysis, P.T., G.Y. and J.Z.; Investigation, H.Z.; Data curation, Z.Z., G.Y. and Y.X.; Writing—original draft, Z.K. Writing—review & editing, Z.K.; Visualization, J.Z.; Supervision, Y.X.; Project administration, H.Z. and J.Z. All authors have read and agreed to the published version of the manuscript.

Data Availability Statement: Not applicable.

References

1. Bou-Mosleh, C.; Rahme, P.; Beaino, P.; Mattar, R.; Nassif, E.A. Contribution to clean energy production using a novel wave energy converter: Renewable energy. In Proceedings of the International Conference on Renewable Energies for Developing Countries 2014, Beirut, Lebanon, 26–27 November 2014; pp. 108–111.
2. Qiu, S.; Zhao, W.; Zhang, C.; Shek, J.K.; Wang, H. A Novel Structure of Tubular Staggered Transverse-Flux Permanent-Magnet Linear Generator for Wave Energy Conversion. *IEEE Trans. Energy Convers.* **2022**, *37*, 24–35. [CrossRef]

3. Ghaheri, A.; Afjei, E.; Hossein, T. Design optimization of a novel linear transverse flux switching permanent magnet generator for direct drive wave energy conversion. *Renew. Energy* **2022**, *198*, 851–860. [CrossRef]
4. Cheng, Y.; Chau, M.; Tong, K. Linear primary permanent magnet vernier machine for wave energy conversion. *IET Electr. Power Appl.* **2015**, *9*, 203–212.
5. Huang, L.; Yu, H.; Hu, M.; Zhao, J.; Cheng, Z. A Novel Flux-Switching Permanent-Magnet Linear Generator for Wave Energy Extraction Application. *IEEE Trans. Magn.* **2011**, *47*, 1034–1037. [CrossRef]
6. Huang, L.; Yu, H.; Hu, M.; Liu, C.; Yuan, B. Research on a Tubular Primary Permanent-Magnet Linear Generator for Wave Energy Conversions. *IEEE Trans. Magn.* **2013**, *49*, 1917–1920. [CrossRef]
7. Zhao, L.; Lu, Q. A Novel Tubular Partitioned Stator Flux-Reversal Permanent Magnet Linear Machine for Direct-Drive Wave Energy Generation. *IEEE Trans. Magn.* **2019**, *55*, 7502707. [CrossRef]
8. Du, Y.; Chau, K.T.; Cheng, M.; Fan, Y.; Wang, Y.; Hua, W.; Wang, Z. Design and Analysis of Linear Stator Permanent Magnet Vernier Machines. *IEEE Trans. Magn.* **2011**, *47*, 4219–4222. [CrossRef]
9. Zhao, M.; Zhang, Z.; Zhang, H.; Xu, Y.; Zou, J. Design and Optimization of Tubular Linear Vernier Generator for Direct Drive Wave Energy Converter. In Proceedings of the 2021 13th International Symposium on Linear Drives for Industry Applications (LDIA), Wuhan, China, 1–3 July 2021; pp. 1–6.
10. Gao, Y.; Qu, R.; Li, D.; Chen, F. Force Ripple Minimization of a Linear Vernier Permanent Magnet Machine for Direct-Drive Servo Applications. *IEEE Trans. Magn.* **2017**, *53*, 7001905. [CrossRef]
11. Zhao, W.; Ma, A.; Ji, J.; Chen, X.; Yao, T. Multiobjective Optimization of a Double-Side Linear Vernier PM Motor Using Response Surface Method and Differential Evolution. *IEEE Trans. Ind. Electron.* **2020**, *67*, 80–90. [CrossRef]
12. Lei, G.; Xu, W.; Hu, J.; Zhu, J.; Guo, Y.; Shao, K. Multilevel Design Optimization of a FSPMM Drive System by Using Sequential Subspace Optimization Method. *IEEE Trans. Magn.* **2014**, *50*, 7016904. [CrossRef]
13. Lee, S.; Kim, Y.; Lee, K.; Kim, S. Multiobjective Optimization Design of Small-Scale Wind Power Generator With Outer Rotor Based on Box–Behnken Design. *IEEE Trans. Appl. Supercond.* **2016**, *26*, 5202605. [CrossRef]
14. Zhu, X.; Yan, B.; Chen, L.; Zhang, R.; Quan, L.; Mo, L. Multi-Objective Optimization Design of a Magnetic Planetary Geared Permanent Magnet Brushless Machine by Combined Design of Experiments and Response Surface Methods. *IEEE Trans. Magn.* **2014**, *50*, 8204004. [CrossRef]
15. Feng, Y.; Zhao, J.; Dong, F.; He, Z.; Song, J. Optimal design of permanent magnet linear synchronous generators at multispeed based on particle swarm optimization combined with SN ratio method. *IEEE Trans. Energy Convers.* **2018**, *33*, 1943–1954.